Heliyon 9 (2023) e20539

Contents lists available at ScienceDirect

Heliyon

journal homepage: www.cell.com/heliyon

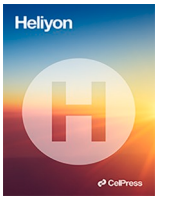

Employing spatial, hybrid and amplitude roughness parameters for unveiling the surface roughness features of mineral and organic admixtures

David Sinkhonde

Department of Civil and Construction Engineering, Pan African University Institute for Basic Sciences, Technology and Innovation, Nairobi, Kenya

ARTICLE INFO

Keywords:
Spatial parameters
Hybrid parameters
Amplitude parameters
Scanning electron microscopy
Amplitude density function
Bearing ratio curve

ABSTRACT

Scanning electron microscopy (SEM) permits to evaluate the surface morphology and surface roughness of pozzolans and admixtures. The field of mineral and organic admixtures has considerable interest in using SEM. However, several challenges are encountered which hamper the precision of quantitative roughness evaluation of mineral and organic admixtures using SEM and these challenges are usually bypassed in literature. In this research, surface roughness properties of pozzolans and admixtures were analysed from six perspectives: spatial parameters, hybrid parameters, amplitude parameters, surface roughness profiles, bearing ratio curves (BRCs) and amplitude density functions (ADFs). The generated roughness characteristics provided detailed information of roughness properties of the pozzolans and admixtures in a time efficient and cost effective way, which is usually very hard to achieve using experimental works. The comparisons of the obtained roughness data for the specimens showed considerable agreement with the roughness profiles and verified the interpretation of the established roughness profiles. Using the ADFs and BRCs for evaluating heights of the roughness profiles provided significant data encapsulated in the shapes of ADFs and BRCs. Moreover, the interpretation of the transformed logarithmic profiles seemed to have nearly retained similar meanings with the conventional profiles, although their scrutiny was observed to be complex. With brand new discussions on spatial, hybrid and amplitude parameters of mineral and organic admixtures, this research is a step forward in characterisation of roughness parameters of mineral and organic admixtures. This study expands the characterisation of pozzolans and admixtures, highlighting significant parameters to be considered in the application of mineral and organic admixtures.

1. Introduction

Characterisation of surface roughness of mineral and organic admixtures is, to a great extent still not clear, and how to interpret the surface roughness parameters' phenomena for pozzolans and admixtures is also an open subject. Improved measurement methods of surface roughness of materials occasion from the demand for quantification of new parameters [1]. The improvements demanded could either be in the processing of material or the technique of obtaining the required information [2]. Engineering needs reliable methods of determining the variables appropriate in characterising the behaviour of materials [3]. It is reported that amplitude parameters for surface roughness such as root mean square roughness (R_q), average roughness (R_a), average waviness (W_a) and root mean

E-mail address: sinkhonde.david@students.jkuat.ac.ke.

https://doi.org/10.1016/j.heliyon.2023.e20539
Received 26 June 2023; Received in revised form 26 July 2023; Accepted 22 September 2023
Available online 30 September 2023

square waviness (W_q) can be used in characterising the roughness properties of mineral and organic admixtures [4]. Nevertheless, heterogeneities in material properties of mineral admixtures could play a role in the variability of material properties and could therefore necessitate additional roughness parameters including spatial and hybrid parameters [5]. A particular scenario is noticed with R_a value. Although the R_a value is the most frequently used parameter in characterising surface roughness, it does not tell the entire story regarding surface roughness [5]. Since R_a is just the area existing between the centre of roughness profile and the profile itself, there is a possibility that some surface profiles could differ in shapes but at the same time have the same R_a values [5]. In such case, finding a solution on surface roughness is not straightforward and it does suffer the serious disadvantage of generating false solutions. The next candidate roughness parameter is R_q but it fails miserably in differentiating the spacing, valleys and peaks of profiles [5]. This is due to the fact that R_a and R_q are both insensitive to differences of spacing, valleys and peaks of the profiles and could result in misleading findings. Based on this experience, the choice of amplitude parameters such as R_a and R_q could be suggested to be suitable for surface characterisation in cases when the effect of heterogeneities on surface roughness vanishes. Given that most shapes of surface roughness are complicated, additional sophisticated roughness parameters are required to obtain useful information about surface roughness.

Since amplitude, spatial and hybrid parameters for characterising surface roughness of mineral and organic admixtures are not well recognised in general literature, employing these parameters could be a cornerstone in such characterisation. Several parameters in characterising roughness of materials have been introduced in order to respond to either quality control or predicting functional features of surfaces (this perhaps being the more important one) [6]. Fortunately, surface roughness can surely be applied in construction industry apart from transport solutions of road surfaces, wood industry and engineering companies [7]. Quantitative surface roughness characterisation, despite its major application being in machining process, has also helped investigators in dealing with civil engineering works including asphalt pavement surfaces and concrete [8,9]. Although the use of surface roughness has been validated in civil engineering, researchers have not paid attention to the estimation of spatial, amplitude and hybrid parameters of pozzolans and admixtures. Depending on fineness, surface texture and particle shape, it is vital to keep in mind that the utilisation of mineral admixtures can decrease or increase the demand of water [10]. In spite of several characterisations of surface texture and roughness of mineral admixtures existing in literature [4,11–17], one [4], has proven to be reasonable in quantitative characterisation of surface roughness. While quantitative evaluation of surface roughness of mineral admixtures has been reported in the foregoing study, spatial and hybrid parameters were entirely neglected. The SEM method in many of these studies are still well-applicable in evaluating the surface texture of mineral admixtures, but cannot be seen as a decisive technique in quantitative evaluation of surface roughness. With brand new discussions on amplitude, spatial and hybrid parameters of mineral and organic admixtures, this study is a step forward in evaluating practical applications of roughness parameters on mineral admixtures. Owing to the multi-wavelength and random elements of surfaces, parametric characterisation of spatial attributes of surfaces is more difficult compared with amplitude features [18]. Based on experimental and mathematical evidence, the hybrid parameters comprise the spatial and amplitude parameters [18]. Despite the difficulty in surface characterisation using spatial parameters, they appear to be an appropriate choice for surface characterisation. Experimental findings of surface roughness characterisation have demonstrated that the spatial and hybrid parameters are important functionally in roughness characterisation [18].

The quality of mineral and organic admixtures can be established based on surface roughness and texture. It should be mentioned that the method of preparing the materials manifests surface roughness character of such materials [9]. It must be mentioned about a commonly known characterisation process of surface morphology, texture and roughness of mineral admixtures using scanning electron microscopy (SEM) reported in literature [13–16,19–22], which is similar to atomic force microscope (AFM), but leaves the quantitative surface roughness parameters out of sight. Examining the details of mineral admixtures using SEM has turned out to be limited for measurements of surface roughness parameters since the method is usually based on qualitative assessment [23]. Consequently, the use of algorithms built in open source Gwyddion is indeed the simplest but necessary extension of SEM in quantitative assessment of surface roughness, as neither spatial roughness parameters nor hybrid roughness parameters could be successfully quantified using SEM only. Apparently, there are several roughness parameters mentioned in literature and it is vital to carefully scrutinise these roughness parameters and select them wisely [1]. Depending on the use of the roughness parameters, it is important to keep in mind that not all roughness parameters are relevant and parameters should be adopted with serious research [24]. Since surface roughness characterisation cannot fully benefit from all roughness parameters, the adoption of selected spatial, amplitude and hybrid parameters in this study proved to be relevant in the characterisation of mineral admixtures.

It is interesting to note that burnt clay powder (BCP), rice husk ash (RHA), cassava starch (CS), gum Arabic (GA) and coconut shell ash (CSA) can be used as either pozzolans or admixtures in concrete production. Accurate characterisation of such specimens can recover solutions of waste management and sustainable construction. There exists a remarkable similarity between surface roughness of mineral and organic admixtures and sustainable construction. Utilising this set of mineral and organic admixtures could resolve the challenges of waste dumping and CO_2 emissions in addition to promoting sustainable construction [25–31]. From production standpoint, there is high production of rice, gum Arabic, coconuts, clay bricks and cassava in the world. Consider Kenya for instance. It is reported that there are high productions of rice husks, cassava, coconut shells and waste clay bricks in Kenya due to its increasing urbanisation [32,33]. Besides, Kenya currently produces approximately 400 metric tonnes of gum Arabic per annum, despite having the potential of generating 12, 000 tonnes per annum. With such high productions, rice husks, gum Arabic, coconut shells, waste clay bricks and woody cassava shrub (Manihot esculenta Crantz) could result in positive results when incorporated in concrete production, fortunately. There is large potential of utilising these pozzolans and admixtures in concrete production. It is on this reason that the mineral and organic admixtures used in this study were collected in Nairobi, Kenya for surface roughness characterisation. At this point, such products can be exploited to generate RHA, CSA, GA, CS and BCP which when in powder form could be utilised as pozzolans and admixtures. Although these pozzolans and admixtures have attractions in concrete production, they suffer from insufficient

characterisation and inability to adequately characterise the actual spatial and hybrid roughness parameters. Much simpler methods of spatial and hybrid parameters, obviously acceptable by several researchers, involve quantitative values of surface roughness. Also, it can involve restructuring of the height profiles generated and such careful restructuring could be plotting bearing ratio curves, amplitude density functions and log transformations.

The main illustration of this research is the diversity of characterisation techniques including spatial, amplitude and hybrid parameters that are to be resorted to so as to obtain quantitative findings from surface roughness of mineral and organic admixtures. Another major illustration is that there is a possibility of characterising the surface roughness of mineral and organic admixtures using bearing ratio curves (BRCs) and amplitude density functions (ADFs). It is anticipated that the contribution from this research will assist in such awareness thereby generating solutions to roughness features of mineral and organic admixtures. It is not reasonable to imagine that only R_a, R_q, skewness (R_{sk}) and kurtosis (R_{ku}) are sufficient to characterise the surface roughness of materials. These parameters although ideal in some surface characterisation of materials in literature [4,18,34–37], are hardly practical in cases of differentiating the spacing, valleys and peaks of the profiles. This is exacerbated further if the shapes of the surfaces are more complicated and the functions of the surfaces are more critical [5]. To resolve this challenge, other useful parameters are required and it is suggested that this would relieve the roughness measurement challenges considerably. It is surprising to note how much vital information regarding surface roughness features of mineral and organic admixtures could be captured using spatial and hybrid roughness parameters. At present, little is known regarding the surface roughness parameters of mineral and organic admixtures and such parameters are worthy of study.

2. Materials and methods

2.1. Raw materials

The materials that were used for experimental and analytical works in this study comprised ordinary Portland cement (OPC) CEM I, BCP, RHA, CS, GA and CSA. Waste clay bricks, coconut shells, cassava starch, rice husks and gum Arabic were outsourced within Nairobi, Kenya. BCP was generated using ball mill erected in the Department of Mechanical Engineering at Jomo Keyatta University of Agriculture and Technology (JKUAT). Generating RHA and CSA involved thermal processing using a furnace. GA procured from Nairobi was crushed to powder form before sieving. On the other hand, CS was produced from cassava cultivated within Kenya. It should be emphasised that specimens passing through 75 μm were generated to enable sufficient information.

2.2. Methods

2.2.1. Material characterisation

The essential properties associated with the generated specimens encompassed specific gravity, chemical compositions, loss on ignition (LOI) and the physicochemical compositions. For the sake of brevity, the detailed procedures and descriptions of the tests are discussed in the author's former publication [4].

2.2.2. Scanning electron microscopy

The morphological properties of the specimens were achieved using SEM. It should be noted that it is more convenient to assess the morphological measurements of specimens using SEM [27,38–42]. Fig. 1 shows a JEOL NeoScope JCM-7000 SEM machine and its structure utilised in this study. Current practice suggests that SEM is one of the most utilised evaluation techniques for solid objects and

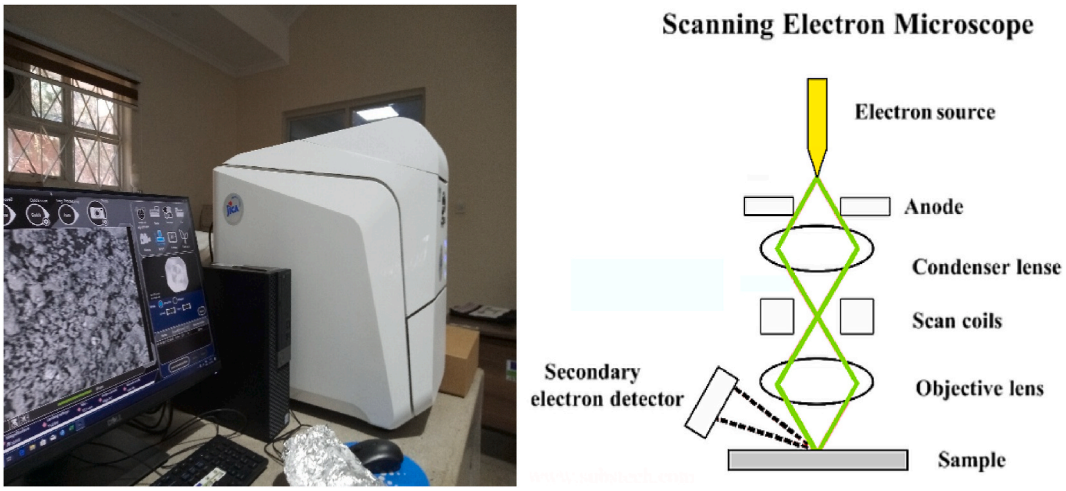

Fig. 1. SEM measuring instrument (left) and its structure (right).

powders [43,44]. Because of the fact that the electrons from SEM interact with sample atoms, the SEM tests require advanced levels of resolution. The general tendency during the assessment of morphology is to (1) dry and clean the specimens to increase surface exposure, (2) sprinkle the specimens on the adhesive tape and (3) scan the samples with an accelerated electron beam. All the specimens were scanned using the scale of 100 μm. With this constant scale, the chances of the characterisation process of specimens not being comparatively sound were remote.

2.2.3. Analytical method

The SEM micrographs were evaluated by means of methods built in Gwyddion in order to establish surface roughness properties. Gwyddion is a proficient software that is generally used in assessments of various surface characteristics of SEM micrographs [45]. The methods used in this study were computationally demanding via amplitude roughness parameters, spatial roughness parameters, hybrid roughness parameters, amplitude density functions (ADFs), bearing ratio curves (BRCs), transformed roughness profiles and statistical parameters. All the methods employed were developed and implemented in the contexts of evaluating surface roughness properties of the specimens under simulation approaches. Such approaches can be conducted fundamentally and distinct methodologies employed during the evaluation procedures are documented elsewhere [34,46–49].

2.2.3.1. Computations of amplitude roughness parameters

2.2.3.1.1. Maximum height of the profile parameter. The maximum height of the profile parameter, R_t has high sensitivity to the deep scratches or high peaks [5]. This parameter is established as the vertical distance existing between the lowest valley occurring along the length of assessment of the profile and the highest peak. Thus, the sought component of maximum height of the profile is additively composed of two parameters as shown in Equation (1).

$$R_t = R_p + R_v \tag{1}$$

in which R_p is the maximum height of the profile on the top of the mean line situated within the length of assessment and R_v is the maximum depth of the profile under the mean line situated within the length of assessment.

2.2.3.1.2. Mean height of peaks. The mean height of peaks, R_{pm} is defined as the mean of the maximum height of the peaks (R_p) generated for every length of sampling of the assessment length [5]. The R_{pm} can be computed using Equation (2).

$$R_{pm} = \frac{1}{n}\left(\sum_{i=1}^{n}(R_{pi})\right) \tag{2}$$

in which n is the number of specimens along the length of assessment of the profile.

2.2.3.1.3. Mean depth of the valleys. The mean depth of the valleys, R_{vm} is established as the mean of the maximum depths of valleys (R_v) generated for every length of sampling of the assessment length [5]. The sought parameter can be computed using Equation (3).

$$R_{vm} = \frac{1}{n}\left(\sum_{i=1}^{n}(R_{vi})\right) \tag{3}$$

in which n is the number of specimens along the length of assessment of the profile.

2.2.3.1.4. Mean of maximum peak to valley height. The mean of maximum peak to valley height, R_{tm} is established as the mean of all maximum heights of peak to valley situated within the length of assessment of the profile [5]. The parameter is expressed as shown in Equation (4).

$$R_{tm} = \frac{1}{n}\left(\sum_{i=1}^{n}(R_{ti})\right) \tag{4}$$

in which n is the number of specimens along the length of assessment of the profile.

2.2.3.1.5. Mean of the third point height. The mean of the third point height, R_{3z} is defined as the mean of the 5 parameters of third point height i.e. R_{3y1}, R_{3y2}, R_{3y3}, R_{3y4} and R_{3y5}. The parameter is calculated as shown in Equation (5).

$$R_{3z} = \frac{1}{5}\left(\sum_{i=1}^{5}(R_{3yi})\right) \tag{5}$$

2.2.3.1.6. Average maximum height of the profile. This parameter has more sensitivity to the occasional deep valleys or high peaks than R_a [5]. The system of international ISO defines this parameter as the height difference between five lowest valleys within the length of assessment of the profile and the mean of the five highest peaks. The parameter is defined as shown in Equation (6).

$$R_{zISO} = \frac{1}{n}\left(\sum_{i=1}^{n}(R_{pi})\right) \tag{6}$$

2.2.3.2. Computations of spatial roughness parameters

2.2.3.2.1. Mean spacing of profile irregularities. This parameter (S_m) is established as the mean spacing existing between the peaks of the profiles at the average line. The profile peak is the profile highest point between downwards and upwards crossing the mean line. This parameter can be defined using Equation (7).

$$S_m = \frac{1}{n}\left(\sum_{i=1}^{n}(S_i)\right) \tag{7}$$

in which n is the number of profile peaks existing at the mean line.

2.2.3.2.2. Average wavelength of the profile. The average wavelength of the profile measures the spacing between local peaks and valleys considering their individual spatial frequencies and relative amplitudes [50]. This parameter is evaluated using Equation (8).

$$\lambda_a = \frac{2\pi R_a}{\Delta_a} \tag{8}$$

in which Δ_a is the mean slope of the profile and R_a is the arithmetic average height.

2.2.3.2.3. Root mean square (RMS) wavelength. This parameter has similar characteristics like those for average wavelength. The root mean square (RMS) wavelength parameter is the root mean of the spacing measurement between local peaks and valleys, considering their individual spatial frequencies and relative amplitudes. It can be computed using Equation (9).

$$\lambda_q = \frac{2\pi R_q}{\Delta_q} \tag{9}$$

2.2.3.3. Computations of hybrid roughness parameters

2.2.3.3.1. Average absolute slope. This parameter is established as a mean absolute profile slope along the length of assessment. The average absolute slope can be computed using values of all the slopes between every two successive points of the profile, followed by mathematical and numerical computations of the means of such slopes. The mean slope parameter is computed using Equations (10) and (11).

$$\Delta_a = \frac{1}{L}\int_0^L \left|\frac{dy}{dx}\right| dx \tag{10}$$

$$\Delta_a = \frac{1}{n-1}\sum_{i=1}^{n-1}\left(\frac{\delta_{yi}}{\delta_{xi}}\right) \tag{11}$$

2.2.3.3.2. Root mean square (RMS) slope. This parameter is the root mean square of the average profile slope. The formulas for computations of this parameter are shown in Equations (12) and (13).

$$\Delta_q = \sqrt{\frac{1}{L}\int_0^L (\theta(x)-\theta)^2 dx},\ \theta = \frac{1}{L}\int_0^L \theta(x)dx \tag{12}$$

$$\Delta_q = \sqrt{\frac{1}{n-1}\sum_{i=1}^{n-1}\left(\frac{\delta_{yi}}{\delta_{xi}}-\theta_m\right)^2},\ \theta_m = \frac{1}{n-1}\sum_{i=1}^{n-1}\left(\frac{y_i - y_{i-1}}{x_i - x_{i-1}}\right) \tag{13}$$

2.2.3.3.3. Developed profile length. The developed profile length is measured by computing the lengths of individual sections of the profile followed by division of the summation of such lengths by the length of assessment [50]. The formula for computing developed profile length is shown in Equation (14).

$$l_o = \frac{1}{L}\sum_{i=1}^{n} l_i \tag{14}$$

in which l_i is the distance of the line number i within the profile which can be computed using Equation (15).

$$l_i = \sqrt{(y_{i+1}-y_i)^2 + \delta x_i^2} \tag{15}$$

in which l_i is the height of the profile at point number i and δx is the horizontal distance between every two successive points.

2.2.3.3.4. Profile length ratio. This parameter is the profile length normalised by the length of evaluation. This parameter is pivotal in measuring the shape of surface in comparison with the L_o as this is not dependent on the measurement length. The formula for computing profile length ratio is shown in Equation (16).

$$L_r = \frac{L_o}{L} \tag{16}$$

2.2.3.4. Surface roughness profiles

2.2.3.4.1. Amplitude density function. In statistics, the parameter of amplitude density function implies the parameter of probability density. The amplitude density function (ADF) is the representation of the distribution histogram for profile heights [5]. It is determined through plot of the density of the profile heights along the horizontal axis and profile heights along the vertical axis. The computation of the density of profile heights involves division of the amplitude scale into reduced sections δ_y. The measurements of the values of amplitude within the δ_y are conducted by computing all values of amplitude existing between δ_y and y in relation to the length of assessment of the profile. The ADF is found using Equation (17).

$$p(y) = \lim_{\delta_y \to 0} \frac{P(y, y + \delta_y)}{\delta_y} \tag{17}$$

For the surface that is generated using a true random procedure, the ADF could be a Gaussian distribution of the heights determined by Equation (18).

$$\mathrm{ADF}\,(y) = \sqrt{2\pi {R_q}^2} \exp\left(\frac{-y^2}{2{R_q}^2}\right) \tag{18}$$

2.2.3.4.2. Bearing ratio curve. The bearing ratio curves are formulated using the ADFs and they are the integrals of the ADFs (from the top down direction). The BRCs are also called the material ratio curves or the Abbott-Firestone curves or the bearing area curves. The BRCs provide the ratios of materials within the profiles at specific depths in comparison with perfectly flat and smooth profiles.

2.2.3.5. Gaussian estimations and fits of profiles and statistical parameters. Logarithmic profiles of texture, roughness and waviness were formulated in this study (Fig. 2). The Gaussian estimates and fits of the generated profiles were developed in the context of estimating the logarithmic profiles of texture, roughness and waviness. Once the Gaussian estimates and fits were formulated, the statistical parameters in connection with the both the profiles and their estimates and fits were generated. The description of the Gaussian function is given by Equation (19).

$$y = y_0 + a\exp\left[-(x - x_0)^2 / b^2\right] \tag{19}$$

in which y is the logarithmic height value, x is associated with transformed profile length, x_0 and y_0 are the initial parameters associated with x and y axes respectively and a and b are constants.

For later reference, it also seemed convenient to generate the statistical parameters associated with the Gaussian functions. These estimates and fits are certainly worth of study and could establish compact explanation of the generated data [51]. The chi-square formula is given by Equation (20).

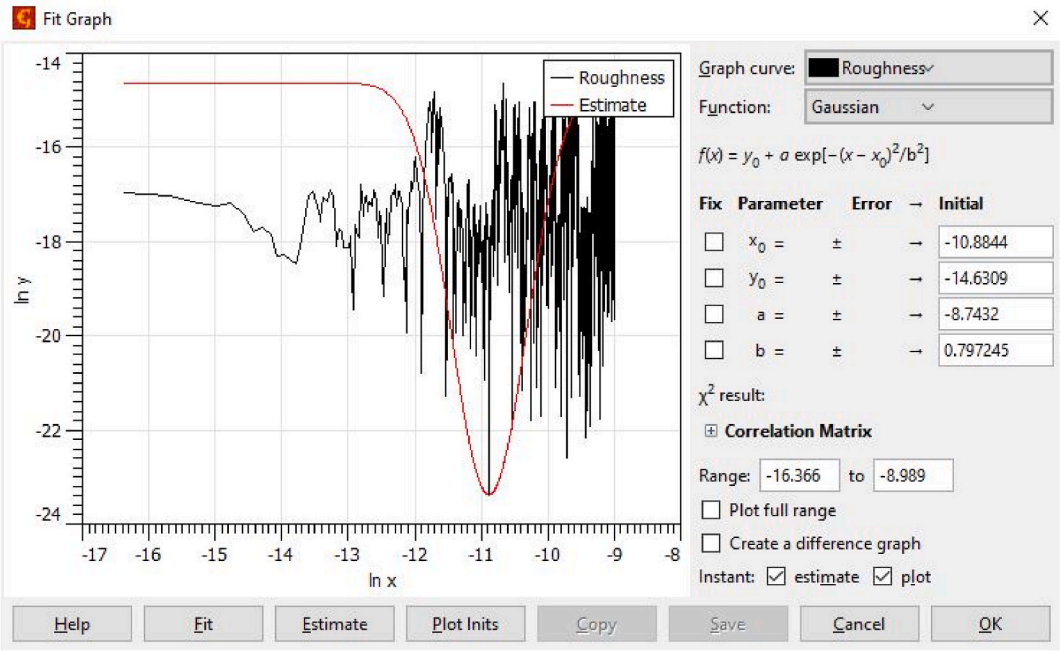

Fig. 2. Snapshot of the process of generating Gaussian estimates and fits of the logarithmic profiles.

$$\chi^2 = \sum_{n=1}^{n} \left(\frac{y_n - f\left(\vec{x}_n; \vec{\theta} \right)}{\sigma_n} \right)^2 \tag{20}$$

in which $\vec{\theta}$ are free parameters of the model, σ_n are the Gaussian errors at positions $\vec{x}_n$, y_n denote the data parameters and n are data values.

If K represents the number of degrees of freedom, the reduced chi-square is obtained by Equation (21). In several cases, the use of reduced chi-square excels in relation with simplicity since its evaluation is based on the comparison to one [52].

$$\chi^2_{red} = \frac{\chi^2}{K} \tag{21}$$

3. Results and discussion

3.1. Characterisation of raw materials

Regarding characterisation of raw materials, it should be noted that the main tests included chemical compositions and physicochemical compositions. The former were aimed at revealing the compliance of BCP, RHA and CSA with pozzolanic specifications in the code [53]. Interestingly, all the investigated specimens complied with the pozzolanic properties specified in such code. The latter were intended at determining the ash, fat, moisture and carbohydrate contents in GA and CS. From the findings, GA and CS were noticed to illustrate substantial amounts of carbohydrates. For further detailed discussion of properties of raw materials, the reader is

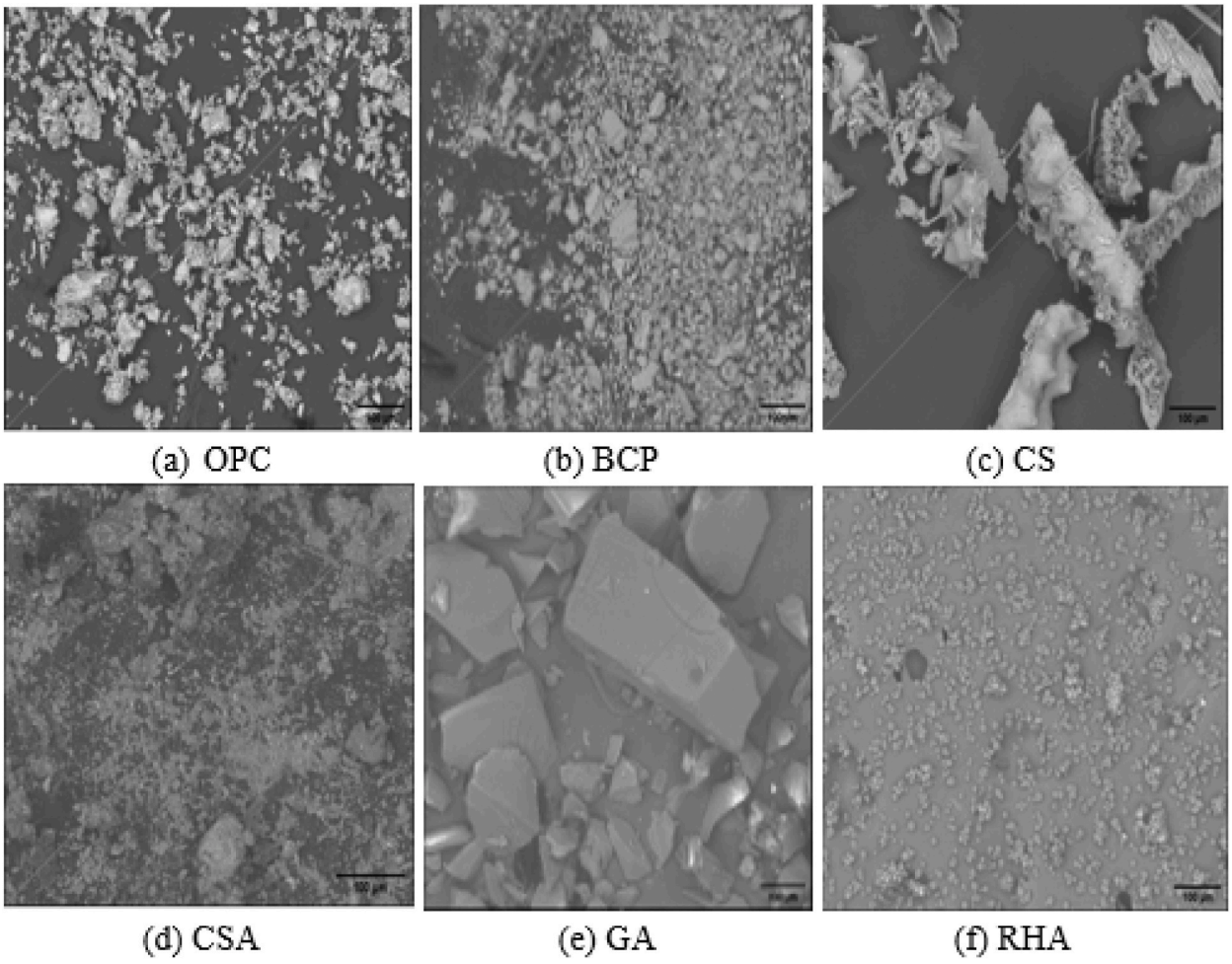

Fig. 3. Generation of SEM micrographs of specimens. The addition of the diagonal line to every SEM micrograph defines the direction in which the spatial, amplitude and hybrid roughness parameters were developed.

referred to the author's former publication [4].

3.2. Scanning electron microscopy

Fig. 3 depicts SEM images of cement, pozzolans and admixtures. The SEM examination allowed particle shapes and surface texture to be analysed, expecting to connect visible surface attributes to quantitative roughness parameters. The development of reliable comparisons among the specimens was based on generating the specimens of mineral and organic admixtures which passed through 75 μm sieve. In addition, the utilisation of high voltage SEM to evaluate the specimens is extremely helpful in establishing significant

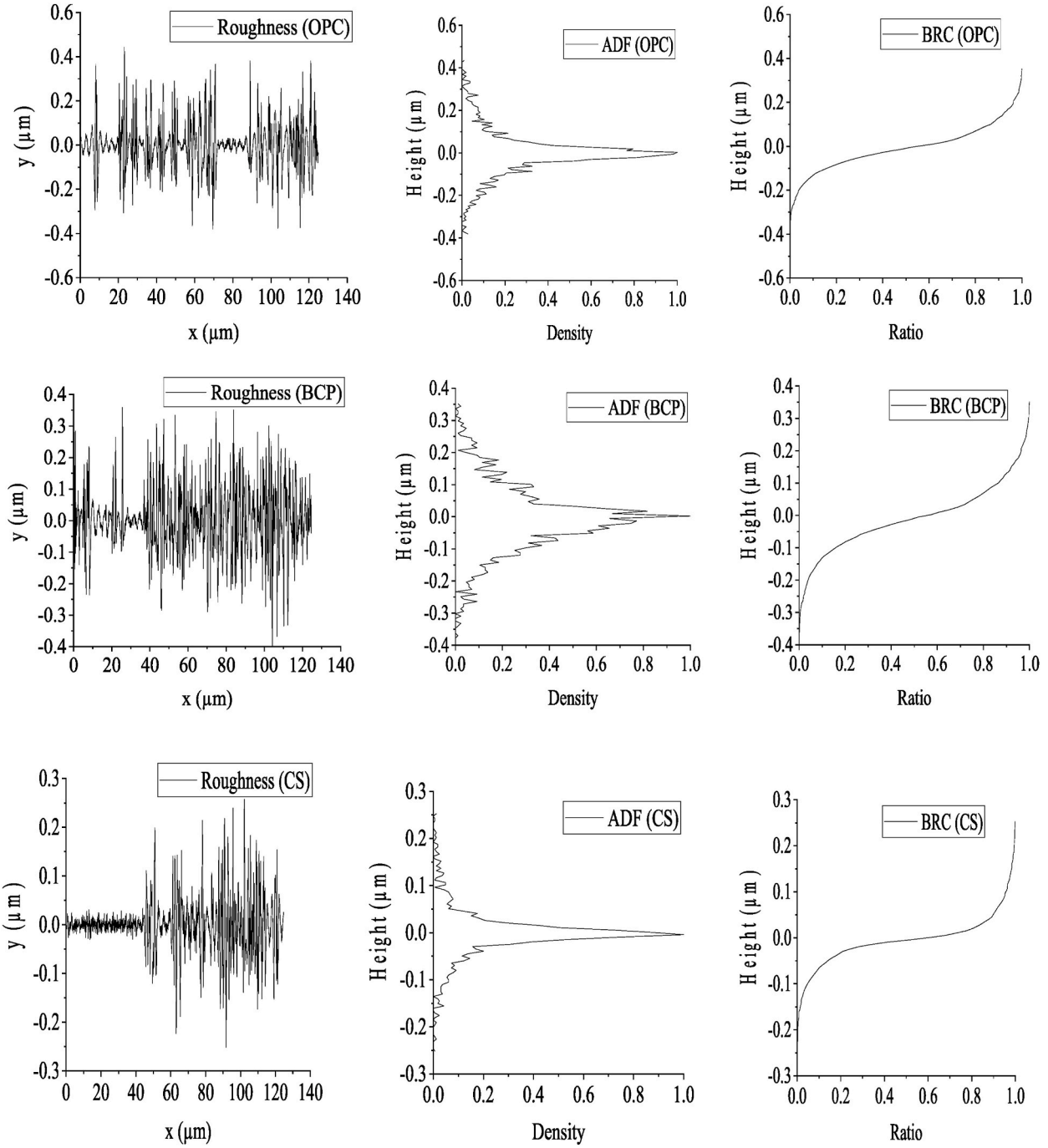

Fig. 4. Dependences of the ADFs and BRCs on the roughness profiles.

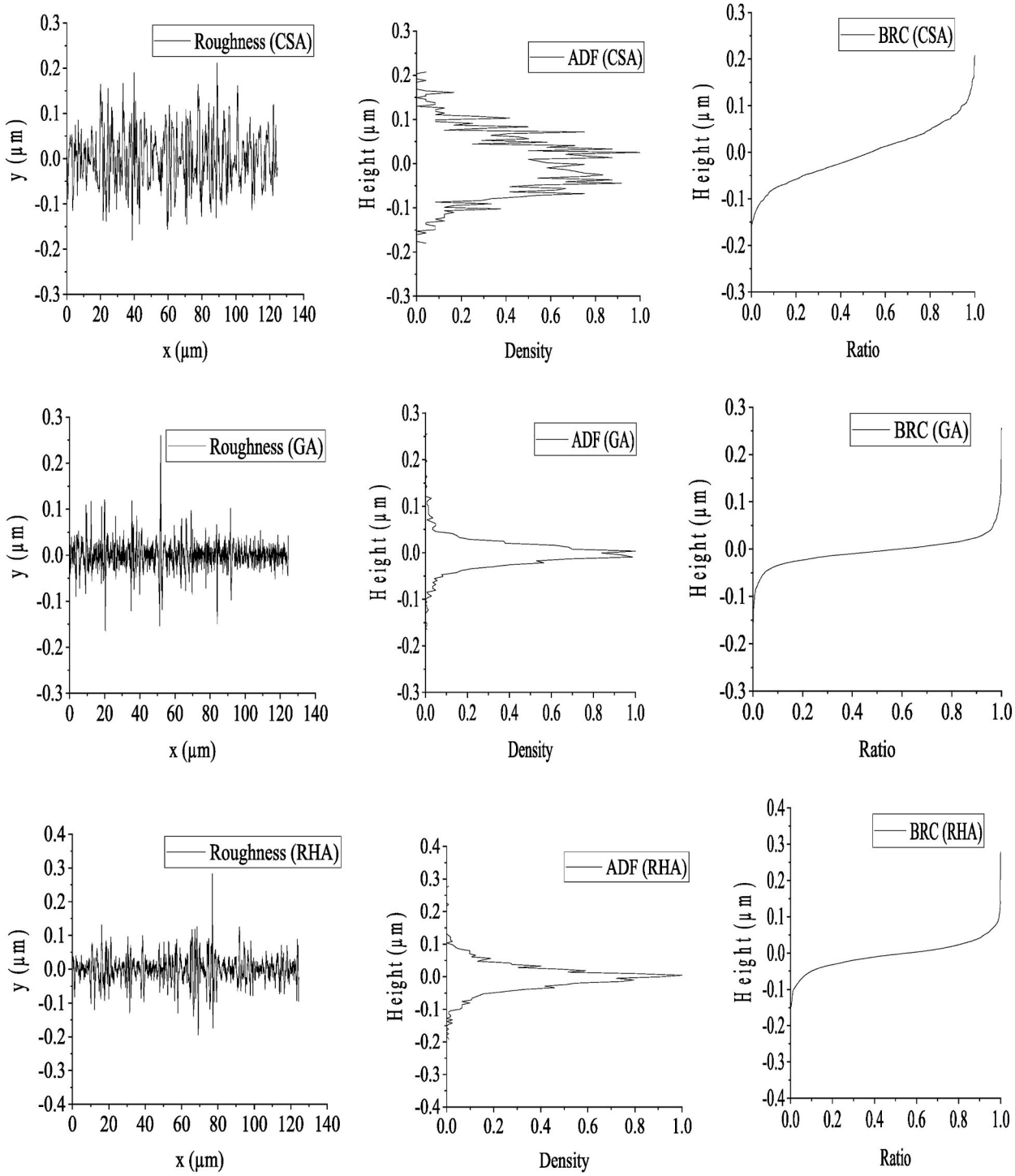

Fig. 4. (*continued*).

data.

Although SEM can evaluate the morphological and structural properties of specimens by scanning the specimens on fine scaling [54,55], it suffers from reduced capability to examine the surface roughness of specimens. To get out of this challenge, alternative procedure, perhaps more realistic, is to compute spatial, amplitude and hybrid parameters. Computation of such parameters seems not to be implementable using SEM only due to its limitation. From the SEM images, roughness properties are evident. Take GA as an example. It seems that the surfaces of GA are characteristically smooth. Although surface roughness of the specimens could be

interpreted to a minimal degree using SEM, within the interpretation could lie confusion since this could be subjective. It is evident that visual observation of the SEM images may dictate the interpretation process. This violates the reliability of the interpretation and is regarded as the principal reason behind subjectivity in such interpretations. On this basis, reliable quantitative procedures have to be introduced. Attempts have been made in this study to improve such surface roughness characterisation to ensure that quantitative values of surface roughness are established. Sufficient roughness parameters were sought in this study to establish a robust surface roughness characterisation. In principle, the use of few roughness parameters in establishing surface roughness of specimens weakens the measurement process of surface roughness [56]. Useful information about amplitude, spatial and hybrid roughness parameters is presented in the subsequent sections.

3.3. Roughness profiles, amplitude density functions and bearing ratio curves

Regarding the extents of roughness of the mineral and organic admixtures, the roughness profiles are depicted in Fig. 4, together with the ADFs and BRCs. Since the roughness profiles are very challenging to interpret, it was planned to improve such interpretation by including the graphs of ADF and BRC. The ADFs and BRCs are better candidates to accomplish more robust and precise estimations of roughness properties of mineral and organic admixtures. Also, having quantitative roughness parameters in Tables 1–3 can be considered as a remarkable step forward in confirming the roughness properties of mineral and organic admixtures. Like several probability distributions, it is observed that all the ADFs for the mineral and organic admixtures have characteristic bell shapes.

From Fig. 4, it is clear that all the surfaces significantly differ both in their geometrical structures, which perhaps result in distinct functionalities in related applications and their appearances. In many sections along the profiles, the curves look too noisy. As a result, interpretation of such profiles using visual assessment would not be very easy. In this research, care was taken not to over rely on the visual observations. Instead, much emphasis was on quantitative findings presented in Tables 1–3. For demonstrative purposes, it can be seen that OPC exhibits the maximum height value, yet its quantitative value cannot be easily identified on the graph. The situation of interpreting the roughness profiles becomes more challenging since the profiles consist of several peaks and valleys which are very close to each other. Consequently, it is impossible to identify distinctions among the surface roughness profiles without simplifications, in which immense care is required.

The ADFs are calculated for the surface roughness profiles, although primary roughness profiles or texture profiles could be utilised in special considerations [5]. The ADF is used to illustrate “how much” of the profile exists at a certain height. In other words, it is the probability which the points within the profiles at selected randomly x values lie at the heights within the reduced neighbourhoods of certain values of z. It is necessary to place the focus on the practical applications of such observation. First, since the root mean square roughness, R_q is a measure of the ADF width, it is concluded that the wider the ADF, the rougher the surface [5]. One must keep in mind that as long as the ADF is wide, the value of R_q is also large. Because the values of root mean square roughness measure the width of ADF, they together manifest the roughness characteristics of materials. Motivated by the previous work by the author [4], recall that the OPC and GA exhibited the highest and lowest R_q values respectively. From what has been said, it can be seen that the ADF width of OPC and the R_q value in the foregoing study are in good agreement. Although there is good agreement between the ADF width and R_q value for OPC, poor agreement between the two parameters is noticed with GA. GA in the foregoing study illustrated the lowest R_q value. Yet, the lowest ADF width in this present study is CSA (data not shown). This situation further complicates the good agreement which existed for OPC. Unfortunately, the cause of this discrepancy was unclear but it can be attributed tentatively to either methodological error or the suggestion that the good agreement between the two parameters cannot be guaranteed. Notwithstanding that there is existence of the discrepancy, the notable discrepancy is not very pronounced, interestingly. Moreover, it could be suggested that further future research is necessary to address this problem.

Now, having the ADFs, it is possible to generate the BRCs. Mathematically, the BRC is the integral function of the ADF from the top to bottom. This is equivalent to mention that the BRC is the corresponding cumulative probability distribution and is highly applied in surface finish [5]. Apparently, the surface topography is established based on values of roughness parameters. Sadly, such values do not provide reflections of functional features of the surfaces [56–58]. Since the values of roughness parameters do not reflect functional features of the surfaces, the BRC can help in solving this shortcoming [58], and in fact, it is possible to visualise with ease the distributions of the heights of valleys and peaks within the profiles. Hence, BRCs are reported to be the powerful guide in instances where it is necessary to introduce particular features in relation to functional requirement and structural integrity for specific applications [2, 58]. It is observed that the heights of the BRCs always coincide with the heights of the roughness profiles of mineral and organic admixtures. In other words, the range of heights for both BRC and roughness profiles practically remain constant for every specimen. As observed in the curves in Fig. 4, every curve has a specific shape established based on the heights of valleys and peaks of the profile from which the BRC was determined. From the graphs, OPC seems to illustrate the maximum height, but this does not give the exact value due to quantitative limitations in Fig. 4. From this experience, measurement data on heights in Table 1 presented hereinafter offer the consistent values for the heights. From the BRCs, GA is observed to illustrate the lowest height of the curve. Reevaluating the height values in Table 1 seems to validate the findings in the BRCs although some inconsistencies could be noticed. While other researchers [2,6], have reported parameters derived from the BRCs (e.g. core roughness depth, R_k, reduced peak height, R_{pk} and reduced valley depth, R_{vk}), these parameters were entirely neglected in this study, as their interpretation requires cumbersome explanations. This falls beyond the scope of this study and studying such parameters is highly recommended in future research works.

3.4. Roughness parameters

The evaluations of roughness parameters defined by Equations (1)–(16), are studied in their influence on surface roughness

parameters of mineral and organic admixtures. In particular, Tables 1–3, enlist the surface roughness parameters generated along the diagonal lines illustrated in Fig. 3. In these evaluation procedures, it was assumed that significant amount of data could be obtained from the diagonal lines of the SEM images. Given the nature of the diagonal lines employed in this research, one could make an obvious conclusion that the sought solutions are reasonable representatives of the entire SEM images. According to other researchers [35, 59–61], the usage of this line could verify the surface roughness of specimens.

3.4.1. Amplitude roughness parameters

Table 1 enlists the values of amplitude roughness parameters computed by Gwyddion. These parameters provide benefit of the capability to define the surface characteristics of the specimens. This could overcome the qualitative assessment of surface roughness of specimens using SEM. Since the parameters in Table 1 are defined using surface profile plots, assessment of such parameters is evaluated with respect to the surface profile plots of the specimens. The general procedure for determining these values involves measurements of such parameters on surface profiles in Fig. 4. However, this procedure can be difficult in cases when the valleys and peaks are very close together. The quantitative values of roughness parameters presented in Table 1, unlike surface roughness profiles presented previously in Fig. 4, are generated with ease without necessity of direct measurements from the profiles. Note that these amplitude parameters adopted in this study are defined by Equations (1)–(6).

Since R_t is the sum of R_p and R_v, it is clear from Table 1, that all values of R_t are the summations of R_p and R_v. This behaviour is encapsulated in Equation (1). R_v values are defined as depths of deepest valleys in the roughness profiles over the evaluation lengths [5]. On the other hand, R_p values are defined as the heights of the highest peaks in the surface profiles over the evaluation lengths [5]. Because of the fact that R_t is the sum of R_p and R_v, it is more convenient to analyse R_t values in details rather than the R_p and R_v values. From Table 1, it is clear that OPC reveals the highest R_t value among the pozzolans and admixtures. A check on this value using the surface profiles in Fig. 4 illustrates that this is indeed true. The lowest R_t value is observed with RHA and its value is marginally lower than that of GA. A negligible percentage reduction of 1.98% is observed for R_t value of RHA compared with that of GA. Notice that a check of the specimen with highest R_t value is simple using Fig. 4 compared with the specimen with lowest R_t value. The reasoning behind this is obviously the negligible percentage reduction of 1.98% for R_t value of RHA in contrast with that of GA. Based on the findings, it is easier to interpret R_t values of the specimens from Table 1 compared with Fig. 4. Although values in Fig. 4 do improve interpretation of amplitude roughness parameters in the sense of providing quantitative values, they do lack details of other heights other than the R_t. This may result in lack of the overall physical meaning of the specimens. The interpretation of quantitative values presented in Table 1 in conjunction with roughness profiles in Fig. 4 overcomes this dilemma by coupling features from both data presentations.

The values of R_{tm} in Table 1 capture the mean parameters and this means that they are averages of the maximum heights of the sample profiles. The R_{tm} values are obtained after the summations of R_{vm} and R_{pm} values. Just as R_t, R_p and R_v values, the R_{tm}, R_{pm} and R_{vm} values offer the advantages of establishing the extremes in the roughness. An interesting concept which could be inferred from the R_{tm} values in Table 1 is that they seem to obey the trend of R_t values despite a minor discrepancy with the R_{tm} value of CSA. The highest R_{tm} value is observed with OPC while the lowest R_{tm} value is noticed with RHA. The values of R_{tm} for BCP, CSA, GA and CS lie within those for OPC and RHA. Although OPC is observed to be the specimen exhibiting the highest R_{tm} value among all specimens, BCP is found to be the specimen showing the highest R_{tm} among the mineral and organic admixtures. It is once again established that the R_{tm} values for CSA, GA, CS and RHA display reduced differences among themselves with the highest difference being 71.436 nm. It can be suggested that the roughness features of CSA, GA, CS and RHA are not substantially different from one another. In contrast, compared with R_{tm} values for OPC, CSA, GA, CS and RHA exhibit the higher R_{tm} margins. Neither of these specimens display differences of less than 258.034 nm in contrast with BCP. Since high R_{tm} values are linked with increased roughness of specimens, there is no serious difficulty in concluding that BCP exhibits the roughest surface among the pozzolans and admixtures. Good agreement exists between the R_{tm} values in Table 1 and Fig. 4. This agreement was foreshadowed in the findings in Fig. 4 where BCP seems to display high peak profile. This roughness property of pozzolans and admixtures imposes variations in properties of cement-based composites. For example, reductions of workability of cementitious composites due to incorporation of BCP and CSA are examples of increased stiffness of cement-based composites occasioning from inclusion of such materials [20,62].

From Table 1, it can be seen that cement reveals the highest ISO R_z accompanied by BCP. Since increased values of ISO R_z imply increased roughness [36], this shows that OPC has the roughest surface among the specimens. It is known that higher R_{3z} values could occasion from surfaces with deep valleys and higher peaks [37]. As explained in Section 3.3, the highest peaks and valleys are seen with OPC as evidenced by increased range of height for y-value. This confirms the highest established R_{3z} value for OPC. Note that R_{3z}

Table 1
Amplitude roughness parameters of pozzolans and admixtures.

Parameter	OPC	BCP	CS	CSA	GA	RHA
Maximum height of the roughness, R_t (nm)	800.439	664.872	508.784	409.128	433.733	425.144
Maximum roughness valley depth, R_v (nm)	412.041	307.842	251.328	179.724	151.454	187.304
Maximum roughness peak height, R_p (nm)	388.398	357.031	257.456	229.404	282.279	237.84
Average maximum height of the roughness, R_{tm} (nm)	697.458	596.081	327.221	338.047	295.671	266.611
Average maximum roughness valley depth, R_{vm} (nm)	339.864	278.789	159.628	154.67	121.326	132.155
Average maximum roughness peak height, R_{pm} (nm)	357.594	317.292	167.593	183.377	174.345	134.456
Average third highest peak to third lowest valley height, R_{3z} (nm)	740.076	627.323	406.53	342.445	289.124	255.252
Average maximum height of the roughness, $R_{z\ ISO}$ (nm)	697.458	596.081	327.221	338.047	295.671	266.611

Table 2
Spatial parameters of pozzolans and admixtures.

Parameter	OPC	BCP	CS	CSA	GA	RHA
Mean spacing of profile irregularities, S_m (nm)	1094.57	896.135	653.551	1640.16	461.863	775.331
Average wavelength of the profile, λ_a (nm)	970.312	841.491	836.357	1650.7	557.557	816.809
Root mean square (RMS) wavelength of the profile, λ_q (nm)	822.864	741.83	846.611	1479.94	602.375	804.263

Table 3
Hybrid parameters of pozzolans and admixtures.

Parameter	OPC	BCP	CS	CSA	GA	RHA
Average absolute slope, Δ_a	0.4688	0.59996	0.265104	0.19547	0.242637	0.222419
Root mean square (RMS) slope, Δ_q	0.803485	0.902719	0.412033	0.27104	0.338787	0.311635
Length, L (μm)	124.781	124.563	124.828	124.652	124.703	124.828
Developed profile length, L_o (μm)	149.823	157.406	133.55	128.914	130.987	130.179
Profile length ratio, l_r	1.20068	1.26367	1.06987	1.03419	1.05039	1.04287

value for BCP in Table 1 reduces by 15.24% compared with that of OPC which is approximately similar to the ISO R_z reduction of 14.54% for the same specimens. One of the interesting components about values of R_{3z} and ISO R_z is that similar trends among the values in Table 1 are observable. The lowest R_{3z} and ISO R_z values are also seen with RHA. It is therefore possible to match findings of R_{3z} and ISO R_z. It is also important to mention that there are various issues that could arise with regard to DIN R_z, in such a way that its implementation needs to be handled with caution. The use of DIN R_z is prone to statistical averages of the local extremes [18]. From the perspective of explaining the extreme properties of surfaces, the adoption of ISO R_z is considered to be more reasonable [18]. Thus, the use of DIN R_z to characterise surface roughness in this study was entirely neglected.

Eventually, a question arose as whether such increased R_{3z} and ISO R_z for BCP could demonstrate any significant meaning to the behaviour of cement-based composites. The rough surfaces of BCP are observed to occasion decreased workability of cement-based composites [62]. It is considered by several researchers [63], that cementitious composites blended with BCP could increase the stiffness of the mixes. Some examples demonstrating the reduced workability of cementitious composites incorporating BCP are presented elsewhere [25,64,65]. On the other hand, although the lowest values of R_{3z} and ISO R_z are observed for RHA, they are marginally lower than those for GA. RHA illustrated reductions of 11.72% and 9.83% for R_{3z} and ISO R_z values respectively, compared with GA. It could be assumed that the roughness features of GA and RHA are similar. In essence, this could be genuinely a valid assumption since the other amplitude roughness parameters discussed earlier also illustrated marginal differences between GA and RHA.

3.4.2. Spatial parameters

In Table 2, the spatial roughness parameters for the specimens are shown. It is noted that the interpretation of surface roughness requires the knowledge of spatial parameters. Based on Equations (7)–(9), the spatial roughness parameters were generated which allowed determination of effective spatial features of the specimens. Since the spatial roughness parameters describing roughness spatially vary, this condition is considered as one of the difficult aspects of assessing surface roughness of specimens [66]. It is obvious that considerations of spatial roughness properties of pozzolans and admixtures can be characterised with the help of mean spacing of profile irregularities, average wavelength of the profile and root mean square (RMS) wavelength of the profile. These parameters are described in details in the subsequent sections.

In the case of mean spacing of profile irregularities, CSA is noticed to be the specimen with highest S_m, λ_a and λ_q values. Just like other amplitude roughness parameters previously presented (R_v and R_{tm}), GA is noticed to illustrate the lowest S_m, λ_a and λ_q values. At first glance, one could suppose that these three spatial roughness parameters could exhibit similar trends since CSA and GA illustrated the highest and lowest spatial roughness values. However, this is not the case as inconsistencies are noticed for the spatial roughness values of the other specimens. In particular, CS, RHA and BCP are noticed to illustrate the second lowest S_m, λ_a and λ_q values respectively. It can be suggested that the utilisation of S_m, λ_a and λ_q values forms the complete system for determination of spatial roughness parameters of the pozzolans and admixtures. Consider the values of S_m for example. With the inclusion of such values in the system, one can obtain the structured roughness surfaces of the specimens [67]. A summary of the findings in Table 2 seems to suggest that there is poorer agreement among the spatial roughness parameters in comparison with amplitude parameters.

Another technique for comparison of the values is to compute the ranges. The ranges for S_m, λ_a and λ_q values among the specimens are found to be 1178.297 nm, 1093.143 nm and 877.565 nm respectively. Although the trends among the spatial roughness parameters are not similar, there seem to be no major distinctions in the ranges. Moreover, it is important to notice that the spatial and amplitude roughness values do not exhibit the similar trends. It seems that the spatial and amplitude roughness parameters could be complementary but some independences could be observed between such parameters. Though this could be debatable, it should be noted that limited studies in literature have gone to great lengths in correlating spatial and amplitude roughness parameters.

3.4.3. Hybrid parameters

With spatial and amplitude details already explained, more data on other roughness parameters are necessary in an attempt to

establish definite conclusions. Significant details on hybrid roughness parameters would shed more light on surface roughness of pozzolans and admixtures. A series of values of average absolute slope (Δ_a), root mean square (RMS) slope (Δ_q), length (L), developed profile length (L_o) and profile length ratio (l_r) have been generated and exhibited in Table 3.

Hybrid parameters are generated from the combination of amplitude parameters and spatial parameters. Using hybrid parameters is considered as an approach that is established based solely on spacing and amplitude [68]. Following averaging of absolute slope, BCP emerged with the highest Δ_a value. The lowest values of Δ_a and Δ_q are noticed with CSA. It should be noticed that the evaluation of values of Δ_a and Δ_q for the specimens reveals similar trends. Given the nature of the interdependences between the Δ_a and Δ_q values, once could generate an obvious conclusion that Δ_q values could be the highest. Comparing Equations (10) and (12), one can also see the dependence of Δ_q values on Δ_a. This behaviour additionally verifies the contribution of Δ_a in the determination of the Δ_q and also

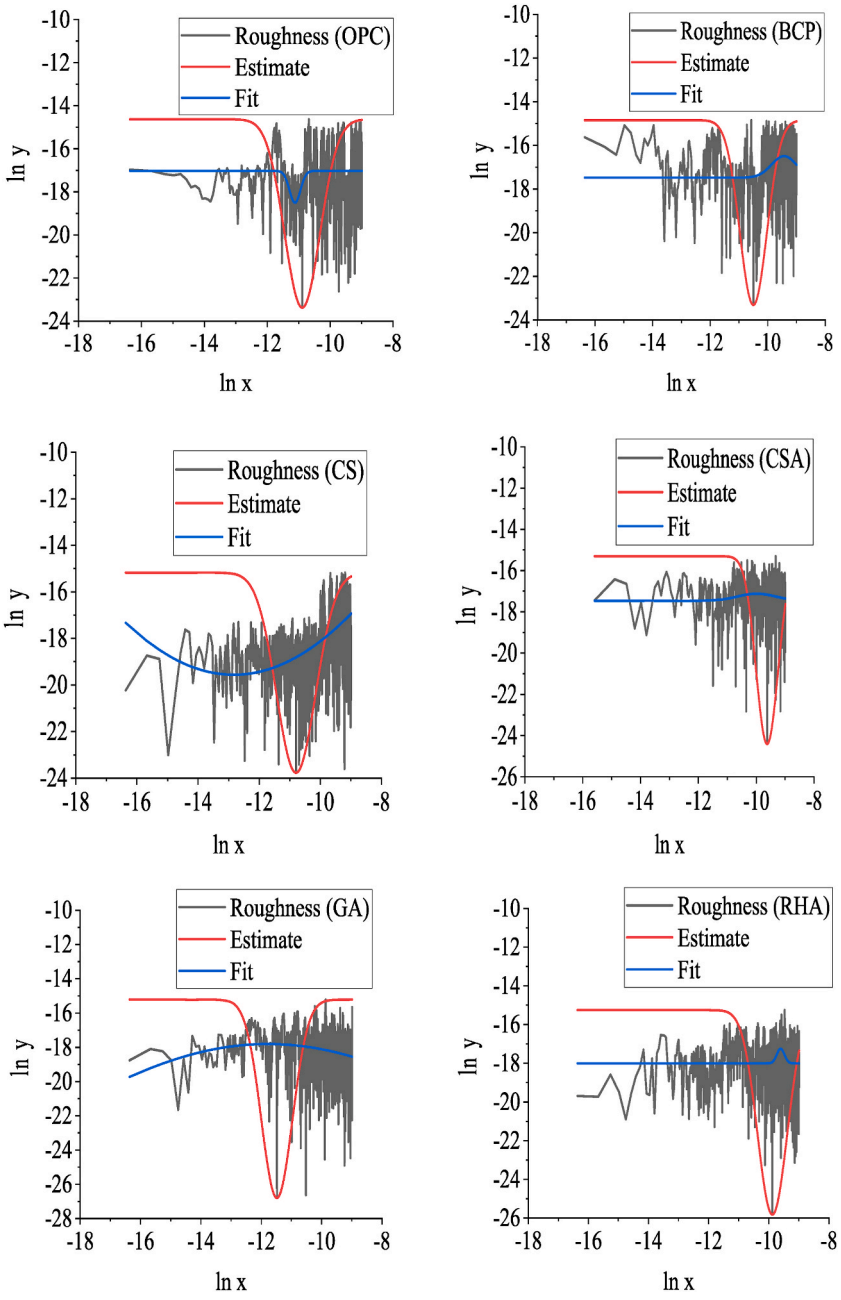

Fig. 5. The logarithmic roughness profiles with Gaussian functions representing the variability of the profiles of the mineral and organic admixtures: (a) Coefficients of determination for fits. OPC: $R^2 = 0.41441$. BCP: $R^2 = 0.60172$. CS: $R^2 = 0.78148$. CSA: $R^2 = 0.78284$. GA: $R^2 = 0.58115$. RHA: $R^2 = 0.51969$. (b) Coefficients of determination for estimates. OPC: $R^2 = 0.84534$. BCP: $R^2 = 0.77699$. CS: $R^2 = 0.87005$. CSA: $R^2 = 0.783$. GA: $R^2 = 0.50308$. RHA: $R^2 = 0.75423$.

Table 4
Statistical parameters from the reconstructed roughness profiles using Gaussian functions.

Statistical parameter	OPC		BCP		CS		CSA		GA		RHA	
	Fit	Estimate	Fit	Estimate	Fit	Estimate	Fit	Estimate	Fit	Estimate	Fit	Estimate
Number of points	1597	1597	1594	1594	1597	1597	734	734	1598	1598	1597	1597
Degrees of freedom	1595	1595	1592	1592	1595	1595	732	732	1596	1596	1595	1595
Reduced chi-sqr	1.63651	0.43222	0.97767	0.54743	0.66637	0.39627	0.508	0.50761	1.08165	1.28328	1.15247	0.58971
Residual sum of squares	2610.229	689.3933	1556.45103	871.5101	1062.853	632.0568	371.8532	371.5713	1726.319	2048.118	1838.194	940.58368
R-square (COD)	0.41441	0.84534	0.60172	0.77699	0.78148	0.87005	0.78284	0.783	0.58115	0.50308	0.51969	0.75423
Adj. R-square	0.41404	0.84524	0.60147	0.77685	0.78134	0.86997	0.78254	0.78271	0.58089	0.50276	0.51939	0.75408

substantiates the surface roughness interpretation employed in this study. It should be mentioned that in case of RMS slope of greater than one, then the topography characterisation of an ultrananocrystalline diamond (UNCD) generated previously by other researchers [69], revealed smooth surfaces. Using the findings from the foregoing study, the specimens in this study could be categorised as rough since all RMS slope values are less than one. However, significant question remains regarding the overall influence of RMS slope values of less than one on the surface roughness features of the specimens. This results in the central challenge in evaluation of surface roughness of specimens with RMS slopes of less than one.

Next, the length, developed profile length and profile length ratio values were generated for all the specimens. The developed profile length is established as an additional parameter for surface roughness characterisation and is worth of consideration in surface profile characterisation [70]. As expected, all the lengths are 125 μm when rounded off to nearest whole number. Likewise, Fig. 4 shows the values of lengths of approximately 125 μm. The differences between the developed profile lengths and the lengths are observed to be small for CS, CSA, GA and RHA. Special attention is paid to the values of profile length ratios which are found to be adequate in the determination of extents of the differences. In the cases of such differences, the profile length values are capable of revealing the percentage reductions in the estimated lengths. With the percentage increments of 6.987%, 3.419%, 5.039% and 4.287% for CS, CSA, GA and RHA respectively, it is obvious that such specimens allowed minor increments in developed profile lengths. The worst case scenario is observed with BCP which reveals the largest increment in developed profile length of 26.367%. It is important to notice that the derivations of the hybrid parameters in Table 3 seem to illustrate some extents of correlation. Consider the largest and lowest values of the hybrid parameters for instance. It is evident that with the exception of length, the values of hybrid parameters for BCP and CSA are the largest and smallest respectively. Good trends are also noticed with the hybrid parameters with the exception of length values. Assuming there are such correlations among the hybrid parameters, it seems reasonable to suggest that one can obtain hybrid roughness parameters with significant relationships among them. This runs contrary to the spatial roughness parameters previously presented which illustrated no significant trends among the investigated specimens. It should also be remarked that the assumed correlation in this study requires substantiation by establishing the correlation between developed profile length and conventional roughness parameters. Further future research is proposed on this interesting concept.

3.5. Roughness profiles

Apart from the conventional roughness profiles, it was necessary to generate the transformed roughness profiles. The challenge with the conventional roughness profiles is that it can oversimplify the roughness measurement processes in the profiles. Fig. 5 plots the ln of height against the ln of x for the roughness profiles. The transformation was performed on both axes. A technique is proposed to estimate the trends of roughness profiles using Gaussian estimates and fits. In this section, mathematical complexity of logarithmic functions is restricted to reduce the ambiguity of the natural log functions. Some rules relating to the logarithmic functions are also thrown in without increasing the ambiguity of the graphs. The magnitudes of coefficients of determination (CODs) of both estimates and the fits are represented in Table 4 in which other statistical parameters have been summarised.

The findings in Fig. 5 demonstrate that the roughness characteristics are considerably adjusted when the profiles undergo logarithmic transformations. The proposed Gaussian functions are used to estimate the transformed profiles of the roughness profiles. So far, this study has approached the assessment of the graphs using quantitative and qualitative descriptions without paying much attention to the many underlying statistics which were generated from these graphs. Only representative statistical parameters have been generated in this paper. As shown in the graphs, it is evident that the transformed roughness profiles for the specimens are similar with the exceptions of CSA and RHA. The transformed roughness profiles of CSA and RHA seem to give a different picture. In instance, the Gaussian estimates for CSA and RHA are noticed to exhibit the curvilinear shapes for ln x values of greater than −11. For values of ln x of less than −11, the Gaussian estimates are characterised by linear graphs. The Gaussian estimates for CSA and RHA at the transitional zones at ln x value of −9 or thereabout do not illustrate any transitional curves. The differences in shapes that these graphs produce are illustrated in Fig. 5. This runs contrary to the transitional zones of the rest of the specimens.

From Fig. 5, height levels of ln y values were considered, which led to approximate height values of the transformed roughness profiles (data not shown). In addition, other height properties of the transformed profiles apart from the maximum height values are ignored in this study since they were not generated. In an attempt to better discuss the correlation between roughness profile heights in Fig. 4 and the heights of the reconstructed profiles in Fig. 5, the heights from both profiles were checked to determine whether the findings differ substantially. Although the largest maximum height of the roughness profiles is noticed with OPC (Table 1 and Fig. 4), the reconstructed logarithmic profiles of GA in Fig. 5 seem to constitute the maximum height level among the specimens. The lowest height of the reconstructed profiles is noticed with CSA whose corresponding height value of the roughness profile in Fig. 4 presents the third lowest value of the six specimens. This situation is not unexpected considering the logarithmic transformation process of the roughness profiles. The impact of transformation or reconstruction of the roughness profiles can be observed in Fig. 5. There seems to be no strong correlation existing between the heights of the roughness profiles in Fig. 4 and the reconstructed profiles in Fig. 5. Indeed, complex logarithmic transformation of roughness profiles induces abrupt modifications in the roughness profiles inasmuch as it has not been commonly reported in literature. It has been demonstrated in this study that the interpretation of the heights of the reconstructed profiles are difficult to capture using the logarithmic scale since it requires cumbersome explanations. On the contrary, the roughness profiles and their corresponding parameters are computationally less demanding as these utilise straightforward calculations, provided the height and length values of the profiles are measured in definite dimensions including nm. Therefore, one must notice that the current method of roughness profile transformation suffers more from inhomogeneities in contrast with the roughness profiles in Fig. 4.

Comparing the profiles, one can see that at the lowest ln y values, lie the transitional zone. Although the transformation generated

using the natural log has attractions, it does suffer from the disadvantage that the shapes of the profiles after the transformation are changed. As expected, there are variations between these transformed roughness profiles and the roughness profiles in Fig. 4. While the roughness profiles in Fig. 4 illustrate OPC as the specimen exhibiting the highest R_t value, these transformed roughness profiles seem to

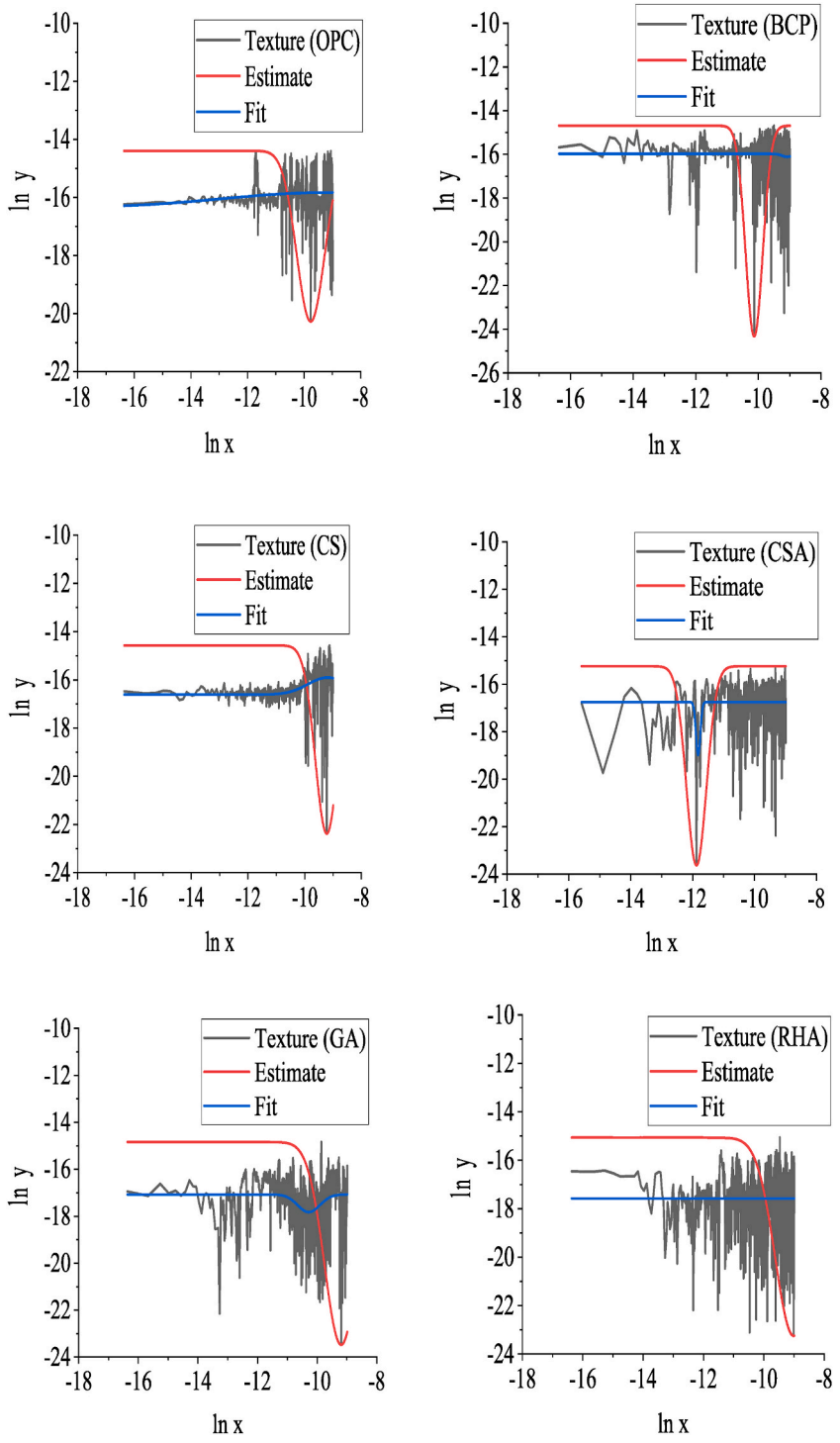

Fig. 6. The logarithmic texture profiles with Gaussian functions representing the variability of the profiles of the mineral and organic admixtures: (a) Coefficients of determination for fits. OPC: $R^2 = 0.71179$. BCP: $R^2 = 0.56783$. CS: $R^2 = 0.73810$. CSA: $R^2 = 0.50968$. GA: $R^2 = 0.59373$. RHA: $R^2 = 0.40023$. (b) Coefficients of determination for estimates. OPC: $R^2 = 0.72547$. BCP: $R^2 = 0.87453$. CS: $R^2 = 0.59888$. CSA: $R^2 = 0.56229$. GA: $R^2 = 0.61582$. RHA: $R^2 = 0.57831$.

Table 5
Statistical parameters from the reconstructed texture profiles using Gaussian functions.

Statistical parameter	OPC		BCP		CS		CSA		GA		RHA	
	Fit	Estimate	Fit	Estimate	Fit	Estimate	Fit	Estimate	Fit	Estimate	Fit	Estimate
Number of points	1597	1597	1596	1596	1597	1597	734	734	1598	1598	1597	1597
Degrees of freedom	1595	1595	1594	1594	1595	1595	732	732	1596	1596	1595	1595
Reduced chi-sqr	0.39874	0.37982	0.76299	0.22151	0.40228	0.61612	0.99352	0.88693	0.88471	0.83659	1.46891	1.03277
Residual sum of squares	635.98305	605.81030	1216.20068	353.08712	641.62920	982.70766	727.26007	649.22956	1412.00107	1335.20231	2342.90535	1647.26619
R-square (COD)	0.71179	0.72547	0.56783	0.87453	0.73810	0.59888	0.50968	0.56229	0.59373	0.61582	0.40023	0.57831
Adj. R-square	0.71161	0.72529	0.56756	0.87445	0.73794	0.59863	0.50901	0.56169	0.59347	0.61558	0.39985	0.57805

illustrate GA as the specimen illustrating the highest ln y value. Apart from the variations in the y-axes for both graphs, there is added difficulty in analysis of numerous peaks and valleys in both Figs. 4 and 5. It should be noted that one of the inherent difficulties is that the Gaussian functions for the profiles in themselves do not seem to be completely satisfactory. This does not imply that they are useless, but the estimates, for example, do not provide feasible estimation of the transformed profiles. Although Gaussian functions have motivated several researchers, it is important to mention that perhaps in future studies other candidate estimation and fitting methods are to be employed. Other functions involving the estimation such as Lorentzian, Boltzmann bent step and smooth slanted step are suspects to provide robust estimation solutions. Notwithstanding this challenge, this study has indicated with the Gaussian functions, it is still hoped that the estimations used herein are considerable estimates of the transformed profiles.

Through the statistical parameters in Table 4, the accuracy of the Gaussian functions are elaborated from distinct perspectives. With the exception of GA, it is clear that the COD values of estimates for the rest of the specimens are greater than their corresponding CODs for the fits. In this study, an explanation to this can be found by examining closely Fig. 5. It can be shown along the fit of reconstructed roughness profile of GA that the increasing COD for the fit was expected in contrast with corresponding COD for the estimate. It can be assumed that for GA, the simplified method that can establish increased COD is just to use the Gaussian fit parameters. The case in which the reduced chi-square is related with the coefficient of determination and adjusted R^2 requires special attention. In this situation, it is considered that an inverse relationship exists between the reduced chi-square and COD. Specifically, the largest COD and adjusted R^2 values are noticed with CSA. On the other hand, CSA illustrates the lowest reduced chi-square value. In another study [71], the model with the lowest reduced chi-square and highest coefficient of determination was selected as best fitting model. It may be suggested that good estimates and fits are the consequences of the high R^2 values and low reduced chi-square values. This justifies the determined relationship between the reduced chi-square and COD. Although there is an inverse relationship between COD and reduced chi-square, the values of number of points and degrees of freedom do not seem to influence the values of COD and reduced chi-square. There is a possibility on the existence of low sensitivity of the COD and reduced chi-square with respect with the degrees of freedom and number of points. Despite the advantages offered by the logarithmic transformation, it seems not to represent well the surface roughness characteristics of the specimens compared with the conventional roughness profiles. The accuracy of the interpretation of the transformed profiles is similar to the roughness profiles, but it is slightly more challenging for surface roughness parameters in contrast with the roughness profiles.

3.6. Texture profiles

In this section, the transformed texture profiles are discussed in details. The transformed texture profiles including their Gaussian functions are elaborated in Fig. 6. These can be used for estimates and fits of the texture profiles. The shapes of the profiles are dramatically adjusted following transformation of the texture profiles. Because of complexity of the curves, the chances of obtaining good Gaussian estimates and fits among the transformed profiles were considered to be very remote. Through the use of statistical parameters in Table 5, detailed information regarding the Gaussian estimates and fits can be accessed.

Just as with transformed roughness profiles previously discussed, the transitional zones of the Gaussian estimates are located at the lowest ln y values for all the specimens with the exception of RHA. The lowest ln y value for RHA seems to coincide with the largest ln x value and hence the Gaussian profile could not be transitioned. Similar to the transformed roughness profiles, the transformations permit the ln values to be negative. This is explicitly the property of natural logarithmic transformations of values less than 1. Since the height values and length values of the profiles were less than 1, these values served this research in demonstrating the ease of the transformation procedures. The key aspect of this transformation is incorporation of logarithmic values as indicators of transformation, which can permit useful information for the texture profiles. The transformed texture profiles together with the Gaussian functions enable distinctions between the profile lengths and the heights following the transformations.

It is evident from Table 5 that the COD values for estimates of the majority of the specimens are greater than the COD values for fits. Only CS exhibits the opposite situation. The study of fits and estimates of CS in Fig. 6 seems to confirm this behaviour. The fit curve for CS is noticed to nicely regularise the texture profile causing the fit curve to be a considerable representative of the texture profile. On the contrary, the estimate curve for CS is observed to substantially diverge from the transformed texture profile values at the beginning up to ln x value of -11. There seems to be a high possibility that this situation might have probably prevented the occurrence of high COD value for the estimate curve. On the other hand, the findings of the estimate curve are seen to nicely overlap with the texture profile values for ln x values greater than -11. Although, the overlap in the latter condition demonstrates the apparent robustness of the estimate of the texture profile, the divergence of the estimate curve from the texture profile in the former condition restrained the occurrence of high COD value for the overall estimate curve. The correlation between the reduced chi-square and COD values is investigated. For higher values of R^2 and adjusted R^2, the reduced chi-square values are seen to reduce. From Table 5, it is explicit that neither of the fits and estimates illustrate COD values of greater than 88%. As a consequence, the use of the Gaussian functions has limitation in the sense that the COD values for the specimens are less than 88% and this situation seemed to have led to higher residual sum of squares of greater than 353. If greater values of residual sum of squares are found, this can mean that fits or the estimates drift away from the texture profiles. Perhaps the use of other functions may help to improve the estimation and fitting processes. While the reduced chi-square values, COD values, adjusted R^2 values and residual sum of square values seem to be related among the tested specimens, the number of points and the degrees of freedom are nearly unaffected by such correlation.

There seem to be inconsistencies existing between the transformed roughness profiles and transformed texture profiles. This is not unexpected because the transformed texture profiles are not similar to the transformed roughness profiles. The effect of transformation of the texture profiles was noticed to be dramatic. Because of the fact that the data for the texture profiles are noisy, the Gaussian estimates and fits are not fully satisfactory. The estimation of noisy data (like those in Fig. 6) with Gaussian functions is increasingly

becoming a challenge and this is common in several areas of study [72]. The selection of Gaussian estimate and fit may or may not be the good choice due to the inaccuracy in estimation of the transformed texture profiles. Also problematic is the closeness of the valleys and peaks of the transformed profiles to one another. This scenario can worsen the accuracy of the estimations and further estimation

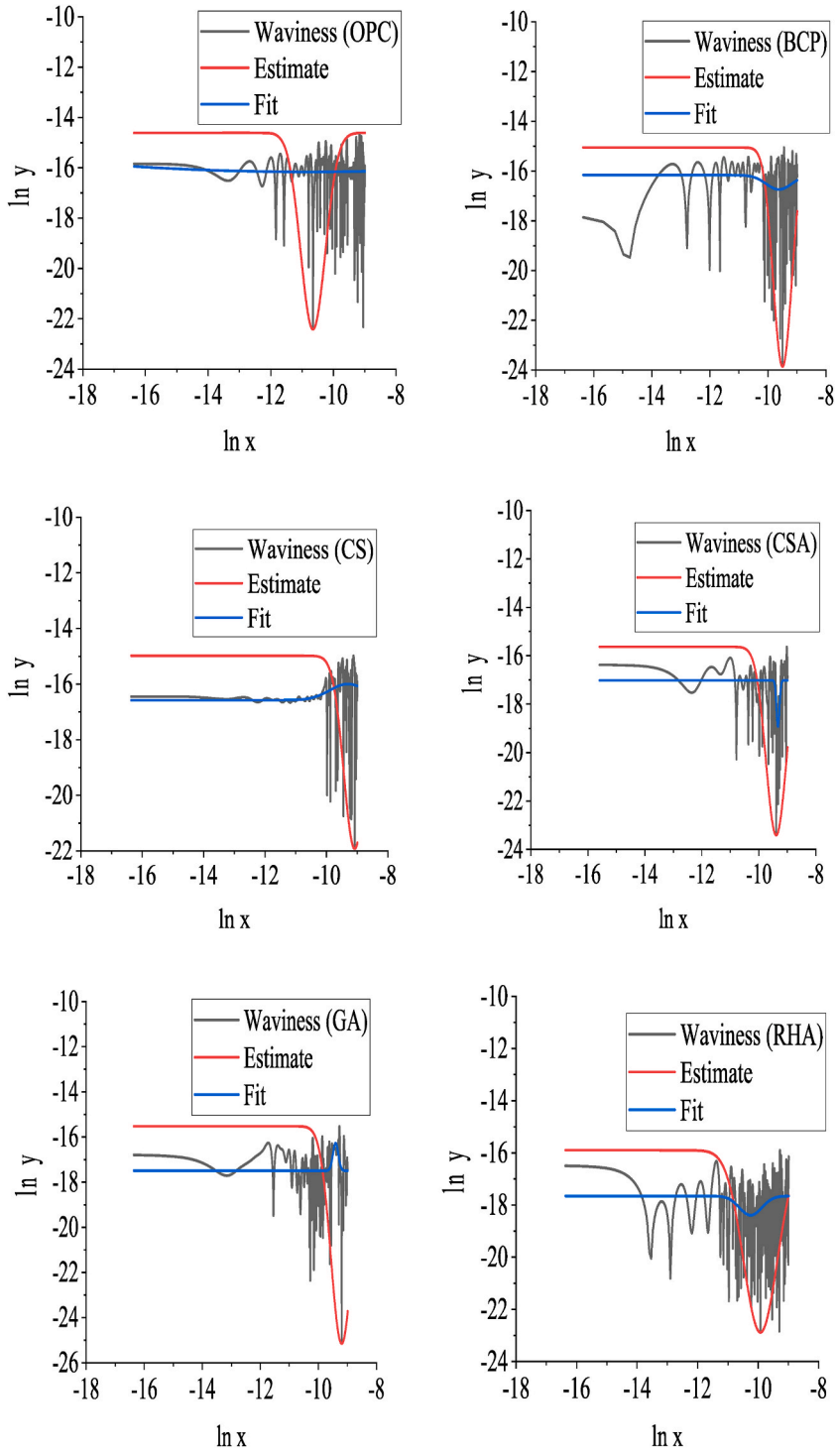

Fig. 7. The logarithmic waviness profiles with Gaussian functions representing the variability of the profiles of the mineral and organic admixtures. (a) Coefficients of determination for fits. OPC: $R^2 = 0.56565$. BCP: $R^2 = 0.55623$. CS: $R^2 = 0.72946$. CSA: $R^2 = 0.69605$. GA: $R^2 = 0.67075$. RHA: $R^2 = 0.54812$. (b) Coefficients of determination for estimates. OPC: $R^2 = 0.85414$. BCP: $R^2 = 0.8472$. CS: $R^2 = 0.71696$. CSA: $R^2 = 0.85406$. GA: $R^2 = 0.74944$. RHA: $R^2 = 0.81541$.

Table 6
Statistical parameters from the reconstructed waviness profiles using Gaussian functions.

Statistical parameter	OPC		BCP		CS		CSA		GA		RHA	
	Fit	Estimate	Fit	Estimate	Fit	Estimate	Fit	Estimate	Fit	Estimate	Fit	Estimate
Number of points	1597	1597	1596	1596	1597	1597	734	734	1598	1598	1597	1597
Degrees of freedom	1595	1595	1594	1594	1595	1595	732	732	1596	1596	1595	1595
Reduced chi-sqr	0.75339	0.253	0.93142	0.32071	0.40667	0.42544	0.58171	0.27931	0.62217	0.47347	0.97317	0.39753
Residual sum of squares	1201.6585	403.5333	1484.68624	511.2187	648.6329	678.5836	425.8143	204.455	992.9808	755.6596	1552.211	634.05475
R-square (COD)	0.56565	0.85414	0.55623	0.8472	0.72946	0.71696	0.69605	0.85406	0.67075	0.74944	0.54812	0.81541
Adj. R-square	0.56538	0.85405	0.55595	0.8471	0.72929	0.71679	0.69563	0.85386	0.67055	0.74928	0.54783	0.8153

functions are to be employed in order to enhance the estimation accuracy. Alternatively, one could choose other functions (e.g. Lorentzian, Boltzmann bent step and smooth slanted step functions), but they must also be assessed in relation to their accuracy in fitting and estimating the transformed texture profiles.

3.7. Waviness profiles

For the waviness profiles of the specimens, it was opted to transform the waviness profiles using logarithmic transformation. This seemed to have proven to be very effective with respect to the interpretation of the profiles, since logarithmic parameters can nearly retain similar meanings with the waviness profiles although their scrutiny can be complex. For the sake of reference, it was decided that the Gaussian estimates and fits be plotted together with the transformed waviness profiles. The generated nonlinear waviness profiles and the Gaussian functions are shown Fig. 7. Table 6 helps in comparing the transformed waviness profiles with estimates and fits through the use of statistical parameters.

The Gaussian functions of the transformed waviness profiles seem to estimate the profiles with fairly good accuracy. The findings of Gaussian functions demonstrate the estimation capabilities of the Gaussian functions on the transformed waviness profiles and they assume the nonlinear behaviour for the large values of logarithmic x scale. The estimation of the reconstructed waviness profiles is approached with linear behaviour. Specifically, the toughest scenario is the nonlinear behaviour and it seems that the Gaussian estimate performs worse in the nonlinear region compared with the linear region. As expected, linear assumptions illustrate several advantages in contrast with the nonlinear ones e.g. ease of numerical implementation [73]. The transitional zones of the Gaussian estimates are located at the lowest ln y values for all the specimens with the exception of CS. It is evident that the lowest ln y value for CS seems to coincide with the largest ln x value and this scenario implied that the Gaussian profile could not be transitioned.

To test the extents of estimates and fits of the waviness profiles, it was necessary to generate the statistical parameters as shown in Table 6. The table demonstrates that the reduced chi-square values, COD values, adjusted R^2 values and residual sum of square values do not seem to be controlled by the number of points and the degrees of freedom. Although strong correlation exists among the former parameters, the latter parameters do not appear to exhibit any strong correlation. Just as with transformed profiles of roughness and texture previously discussed, it has been shown in Table 6 that high values of COD occasion decreased values of reduced chi-square. It appears that Fig. 7 summarises that OPC is the specimen having the highest logarithmic height. On the other hand, CS seems to illustrate the lowest logarithmic height value among the simulated specimens. Despite that nonlinear and linear estimation functions exist for all the simulated specimens, significant distinctions in the shapes of estimation functions can be seen (especially at the transitional zones as previously commented). Such distinctions existing in Fig. 7 are just the consequences of the differences of the waviness profiles reconstructed at nearly the same profile lengths. While this study addressed the significance of Gaussian functions in evaluating the logarithmic waviness profiles, the comparisons of the Gaussian functions used in this study with other functions are entirely neglected. It can also be suggested that additional estimation and fitting functions could improve the accuracy of the profiles, but could also at the same time complicate the estimation and fitting processes.

4. Conclusions

In this paper, the surface roughness properties of pozzolans and admixtures were investigated using spatial, amplitude and hybrid parameters. From the findings, the following conclusions were established.

1. The developed spatial, amplitude and hybrid roughness parameters for solving characterisation of surface roughness of pozzolans and admixtures have allowed significant features of surface roughness to be captured. This approach seems to be an efficient approach in relation to computational time and cost.
2. The generated roughness characteristics provide detailed information of roughness properties of the pozzolans and admixtures in a time efficient and cost effective way which is at times very hard or even impossible to achieve using experimental works.
3. The comparisons of the obtained roughness data for the specimens showed good agreement with the roughness profiles and verified the interpretation of the established roughness profiles.
4. The developed length of profile is considered as an additional important parameter for surface profile characterisation. This parameter together with the profile length ratio, average absolute slope and RMS slope provided reliable quantitative analysis of the profiles.
5. Using the concepts of ADFs and BRCs for evaluating heights of the roughness profiles, characterisation approach of roughness parameters could be extended to advance statistical analyses, which in turn has great prospects in obtaining significant data encapsulated in the shapes of ADFs and BRCs.
6. From the point of view of simplified surface roughness interpretation, roughness, texture and waviness profiles are suggested to be the most promising profiles unlike their corresponding transformed logarithmic profiles. This is primarily connected to the ambiguous interpretation of the transformed logarithmic profiles.
7. The obtained findings could be vital in establishing other methods which can be able to capture the surface roughness of the mineral and organic admixtures. This in turn has great prospects in the evaluation of problems in characterisation of mineral and organic admixtures including the ones studied in this research.

Author contribution statement

David Sinkhonde: Conceived and designed the experiments; Performed the experiments; Analysed and interpreted the data; Contributed reagents, materials, analysis tools or data; Wrote the paper.

Data availability statement

Data will be made available on request.

Declaration of competing interest

The author wishes to confirm that there are no known conflicts of interest associated with this publication and there has been no significant financial support for this work that could have influenced its outcome.

Acknowledgements

The author thanks the Pan African University Institute for Basic Sciences, Technology and Innovation (PAUSTI) for funding. The use of scanning electron microscope (SEM) in the Department of Food Science and Technology at Jomo Kenyatta University of Agriculture and Technology (JKUAT) is acknowledged. The author also acknowledges the valuable comments from reviewers in their busy schedules.

References

[1] D.J. Whitehouse, J.F. Archard, The properties of random surfaces of significance in their contact, Proc. R. Soc. London. A. Math. Phys. Sci. 316 (1524) (1970) 97–121.
[2] D.J. Whitehouse, Assessment of surface finish profiles produced by multi-process manufacture, Proc. Inst. Mech. Eng. Part B J. Eng. Manuf. 199 (4) (1985) 263–270.
[3] A. Fehér, R. Kovács, On the evaluation of non-Fourier effects in heat pulse experiments, Int. J. Eng. Sci. 169 (September) (2021), 103577.
[4] D. Sinkhonde, Quantitative study on surface porosity and roughness parameters of mineral and organic admixtures based on multi-scale characterisation techniques, Clean. Mater. 7 (September) (2022), 100166.
[5] StudyLib, Surface Profile Parameters, 2020 [Online]. Available: https://studylib.net/doc/8113591/. Accessed: 29-Jan-2023.
[6] P. Pawlus, R. Reizer, M. Wieczorowski, G. Krolczyk, Material ratio curve as information on the state of surface topography—a review, Precis. Eng. 65 (2020) 240–258.
[7] D. Kubátová, M. Melichar, Roughness evaluation using abbott-firestone curve parameters, in: 30th DAAAM International Symposium on Intelligent Manufacturing and Automation, 2019, pp. 467–475.
[8] J.C. Wambold, J.J. Henry, *NASA Wallops Tire/runway Friction Workshops: 1993– 2002*. 1911 East College Avenue, State, CDRM Incorporated, College, PA United States 16804, 2002.
[9] P.M.D. Santos, E.N.B.S. Júlio, A state-of-the-art review on roughness quantification methods for concrete surfaces, Construct. Build. Mater. 38 (2013) 912–923.
[10] American Concrete Institute, What Does a Pozzolan Do in the Concrete?, 2020 [Online]. Available: https://www.concrete.org/tools/frequentlyaskedquestions.aspx?faqid=689. Accessed: 08-Aug-2023.
[11] O.M. Sierra, J. Payá, J. Monzó, M.V. Borrachero, L. Soriano, J. Quiñonez, Characterization and reactivity of natural pozzolans from Guatemala, Appl. Sci. 12 (21) (2022).
[12] R. Walker, S. Pavía, Physical properties and reactivity of pozzolans, and their influence on the properties of lime-pozzolan pastes, Mater. Struct. Constr. 44 (6) (2011) 1139–1150.
[13] P.B. Madakson, D.S. Yawas, A. Apasi, Characterization of coconut shell ash for potential utilization in metal matrix composites for automotive applications, Int. J. Eng. Sci. Technol. 4 (3) (2012) 1190–1198.
[14] A. Abuarra, R. Hashim, S. Bauk, S. Kandaiya, E.T. Tousi, Fabrication and characterization of gum Arabic bonded Rhizophora spp. particleboards, Mater. Des. 60 (2014) 108–115.
[15] Z.Q. Huang, J.P. Lu, X.H. Li, Z.F. Tong, Effect of mechanical activation on physico-chemical properties and structure of cassava starch, Carbohydr. Polym. 68 (1) (2007) 128–135.
[16] W. Xu, T.Y. Lo, S.A. Memon, Microstructure and reactivity of rich husk ash, Construct. Build. Mater. 29 (2012) 541–547.
[17] D. Sinkhonde, A. Rimbarngaye, B. Kone, T.C. Herring, Representativity of morphological measurements and 2-d shape descriptors on mineral admixtures, Results Eng 13 (2022), 100368.
[18] W.P. Dong, P.J. Sullivan, K.J. Stout, Comprehensive study of parameters for characterising three-dimensional surface topography: IV: parameters for characterising spatial and hybrid properties, Wear 178 (1–2) (1994) 45–60.
[19] G.C. Cordeiro, R.D. Toledo Filho, L.M. Tavares, E.D.M.R. Fairbairn, S. Hempel, Influence of particle size and specific surface area on the pozzolanic activity of residual rice husk ash, Cem. Concr. Compos. 33 (5) (2011) 529–534.
[20] T.C. Herring, J.N. Thuo, T. Nyomboi, Engineering and durability properties of modified coconut shell concrete, Civ. Eng. J. 8 (2) (2022) 362–381.
[21] D. Mirindi, R.O. Onchiri, J. Thuo, Physico-mechanical properties of particleboards produced from macadamia nutshell and gum Arabic, Appl. Sci. 11 (23) (2021).
[22] B. Kone, J.N. Mwero, E.K. Ronoh, Experimental effect of cassava starch and rice husk ash on physical and mechanical properties of concrete, Int. J. Eng. Trends Technol. 70 (2) (2022) 343–350.
[23] G.W. Stachowiak, A.W. Batchelor, G.B. Stachowiak, Characterization of test specimens, in: Tribology Series, Elsevier B.V., 2004, pp. 115–150.
[24] D.J. Whitehouse, The parameter rash - is there a cure? Wear 83 (1) (1982) 75–78.
[25] Z. Ge, Y. Wang, R. Sun, X. Wu, Y. Guan, Influence of ground waste clay brick on properties of fresh and hardened concrete, Construct. Build. Mater. 98 (2015) 128–136.
[26] B. Liu, J. Quin, J. Shi, J. Jiang, X. Wu, Z. He, New perspectives on utilization of CO2 sequestration technologies in cement-based materials, Construct. Build. Mater. 272 (2021).
[27] K. Ganesan, K. Rajagopal, K. Thangavel, Rice husk ash blended cement: assessment of optimal level of replacement for strength and permeability properties of concrete, Construct. Build. Mater. 22 (8) (2008) 1675–1683.
[28] M.S. Shetty, Concrete Technology: Theory and Practice 55, S. Chand & Company L.t.d., New Delhi, 2000.
[29] M.J. Snyder, H.W. Nelson, A Critical Review of Technical Information on the Utilization of Fly Ash, Battelle Memorial Institute, Ohio, USA, 1962.

[30] A. Vissac, A. Bourges, D. Gandreau, R. Anger, L. Fontaine, Argiles & biopolymères: les stabilisants naturels pour la construction en terre, 2017 [Online]. Available: https://hal.archives-ouvertes.fr/hal-01682536.
[31] D.K. Smith, Utilization of fly ash in the cementing of wells, Soc. Min. Eng. AIME Prepr. (1968) 68. F-17.
[32] U. Kleih, A. Hollingdate, Production of High Quality Rice Husk Ash, Chatham, UK, 1993.
[33] D. Oni, J. Mwero, C. Kabubo, The effect of cassava starch on the durability characteristics of concrete, Open Civ. Eng. J. 14 (2020) 289–301.
[34] S. Zhao, Y. Li, Y. Wang, Z. Ma, X. Huang, Quantitative study on coal and shale pore structure and surface roughness based on atomic force microscopy and image processing, Fuel 244 (January) (2019) 78–90.
[35] C. Jia, J. Lai, W. Chen, Y. Lu, Y. Cai, Y. Liang, Microscopic wettability of medium rank coals involved pore features and functional groups, Nat. Gas. Ind. B 9 (4) (2022) 325–335.
[36] S. Hiziroglu, P. Kosonkorn, Evaluation of surface roughness of Thai medium density fiberboard (MDF), Build. Environ. 41 (4) (2006) 527–533.
[37] W.R. Chang, The effect of surface roughness on the measurement of slip resistance, Int. J. Ind. Ergon. 24 (3) (1999) 299–313.
[38] M. Li, et al., A bioinspired alginate-gum Arabic hydrogel with micro-/nanoscale structures for controlled drug release in chronic wound healing, ACS Appl. Mater. Interfaces 9 (27) (2017) 1–32.
[39] M.M. Al-Ansari, N.D. Al-Dahmash, A.J.A. Ranjitsingh, Synthesis of silver nanoparticles using gum Arabic: evaluation of its inhibitory action on Streptococcus mutans causing dental caries and endocarditis, J. Infect. Public Health 14 (3) (2021) 324–330.
[40] N.L. Thomas, J.D. Birchall, The retarding action of sugars on cement hydration, Cem. Concr. Compos. 13 (1983) 830–842.
[41] K. Gunasekaran, R. Annadurai, P.S. Kumar, Study on reinforced lightweight coconut shell concrete beam behavior under shear, Mater. Des. 50 (2013) 293–301.
[42] K. Gunasekaran, R. Annadurai, P.S. Kumar, Study on reinforced lightweight coconut shell concrete beam behavior under flexure, Mater. Des. 46 (2013) 157–167.
[43] S. Spiegelberg, A. Kozak, G. Braithwaite, Characterization of Physical, Chemical, and Mechanical Properties of UHMWPE, Third Edit. Elsevier Inc., 2016.
[44] N. Raval, R. Maheshwari, D. Kalyane, S.R. Youngren-Ortiz, M.B. Chougule, R.K. Tekade, Importance of Physicochemical Characterization of Nanoparticles in Pharmaceutical Product Development, Elsevier Inc., 2018.
[45] M.Z. Butt, D. Ali, M. Aftab, M.U. Tanveer, Surface topography and structure of laser-treated high-purity zinc, Surf. Topogr. Metrol. Prop. 3 (3) (2015), 35002.
[46] A.L. Carvalho, F. Maugeri, V. Silva, A. Hernández, L. Palacio, P. Pradanos, AFM analysis of the surface of nanoporous membranes: application to the nanofiltration of potassium clavulanate, J. Mater. Sci. 46 (10) (2011) 3356–3369.
[47] H. Yazid, H. Arof, Gradient based adaptive thresholding, J. Vis. Commun. Image Represent. 24 (7) (2013) 926–936.
[48] T. Kimura, Y. Miyato, K. Kobayashi, H. Yamada, K. Matsushige, Investigations of local electrical characteristics of a pentacene thin film by point-contact current imaging atomic force microscopy, Jpn. J. Appl. Phys. 51 (2012), 8 PART 4.
[49] D. Nečas, P. Klapetek, Gwyddion: an open-source software for SPM data analysis, Cent. Eur. J. Phys. 10 (1) (2012) 181–188.
[50] E.S. Gadelmawla, M.M. Koura, T.M.A. Maksoud, I.M. Elewa, H.H. Soliman, Roughness parameters, J. Mater. Process. Technol. 123 (2002) 133–145.
[51] R.A. Poldrack, Statistical Thinking for the 21st Century, Princeton University Press, New Jersey, USA, 2022.
[52] R. Andrae, T. Schulze-Hartung, P. Melchior, Dos and Don'ts of Reduced Chi-Squared, 2010, pp. 1–12.
[53] ASTM C618, Standard Specification for Coal Fly Ash and Raw or Calcined Natural Pozzolan for Use in Concrete, ASTM International, West Conshohocken, USA, 2003.
[54] J.T. Orasugh, S.K. Ghosh, D. Chattopadhyay, Nanofiber-reinforced Biocomposites, 2020.
[55] P. Lin, S. Lin, P.C. Wang, R. Sridhar, Techniques for physicochemical characterization of nanomaterials, Biotechnol. Adv. 32 (4) (2013) 711–726.
[56] D.J. Whitehouse, Surfaces — a link between manufacture and function, Proc. Inst. Mech. Eng. 192 (1) (1978) 179–188.
[57] M. Field, J.F. Kahles, M.F. DeVries, Relationship of surface roughness and surface integrity to functional properties, Int. Inst. Prod. Eng. Res. 25 (2) (1976) 569–573.
[58] M.C. Salcedo, I.B. Coral, G.V. Ochoa, Characterization of surface topography with Abbott Firestone curve, Contemp. Eng. Sci. 11 (68) (2018) 3397–3407.
[59] L.L.G. Al-mahamad, Synthesis and surface characterization of new triplex polymer of Ag(I) and mixture nucleosides: cytidine and 8-bromoguanosine, Heliyon 5 (5) (2019), e01609.
[60] K. Kakaei, M.D. Esrafili, A. Ehsani, Characterization 27 (2019).
[61] A. Sikora, A. Rodak, O. Unold, P. Klapetek, The development of the spatially correlated adjustment wavelet filter for atomic force microscopy data, Ultramicroscopy 171 (2016) 146–152.
[62] D. Sinkhonde, R.O. Onchiri, W.O. Oyawa, J.N. Mwero, Effect of waste clay brick powder on physical and mechanical properties of cement paste, Open Civ. Eng. J. 15 (2021) 370–380.
[63] Z. Bayasi, P. Soroushian, Optimum use of pozzolanic materials in steel fiber reinforced concrete, Transport. Res. Rec. (1990) 25–30.
[64] Civil Engineering Forum, Workability of Concrete and the Factors Influencing its Value, Podgorica, Montenegro, 2020.
[65] C. Patil, Lab Manual of Concrete Technology, Sanjay Chodawat Group, New Delhi, India, 2015.
[66] G.A. Lehrsch, F.D. Whisler, M.J.M. Römkens, Spatial variation of parameters describing soil surface roughness, Soil Sci. Soc. Am. J. 52 (2) (1988) 311–319.
[67] S.G. Kandlikar, Single-Phase Liquid Flow in Minichannels and Microchannels, second ed., no. 1999, Elsevier Ltd, 2013.
[68] Hobson Taylor, What are Hybrid Parameters? (2022) [Online]. Available: https://www.taylor-hobson.com/resource-center/faq/what-are-hybrid-parameters. Accessed: 15-Feb-2023.
[69] A. Gujrati, S.R. Khanal, L. Pastewka, T.D.B. Jacobs, Combining TEM, AFM, and profilometry for quantitative topography characterization across all scales, ACS Appl. Mater. Interfaces 10 (34) (2018) 29169–29178.
[70] V. Radhakrishnan, Significance of profile measurements length in roughness, Wear 23 (1972) 339–347.
[71] P. Pornpraipech, M. Khusakul, R. Singklin, P. Sarabhorn, C. Areeprasert, Effect of temperature and shape on drying performance of cassava chips, Agric. Nat. Resour. 51 (5) (2017) 402–409.
[72] N. Hagen, M. Kupinski, E.L. Dereniak, Gaussian profile estimation in one dimension, Appl. Opt. 46 (22) (2007) 5374–5383.
[73] A. Apolinar-Fernández, J. Barrasa-Fano, M. Cóndor, H. Van Oosterwyck, J.A. Sanz-Herrera, Traction force reconstruction assessment on real three-dimensional matrices and cellular morphologies, bioRxiv 186 (June 2022) (2022), 2022.11.16.516745.